

# Vision Transformers for Multi-Variable Climate Downscaling: Emulating Regional Climate Models with a Shared Encoder and Multi-Decoder Architecture

Fabio Merizzi<sup>1\*</sup> and Harilaos Loukos<sup>2</sup>

<sup>1</sup>Department of Informatics: Science and Engineering (DISI), University of Bologna, Mura Anteo Zamboni 7, Bologna, 40126, Italy .

<sup>2</sup>The Climate Data Factory (TCDF), Paris, France .

\*Corresponding author(s). E-mail(s): [fabio.merizzi@unibo.it](mailto:fabio.merizzi@unibo.it);

## Abstract

Global Climate Models (GCMs) are critical for simulating large-scale climate dynamics, but their coarse spatial resolution limits their applicability in regional studies. Regional Climate Models (RCMs) refine this through dynamic downscaling, albeit at considerable computational cost and with limited flexibility. While deep learning has emerged as an efficient data-driven alternative, most existing studies have focused on single-variable models that downscale one variable at a time. This approach can lead to limited contextual awareness, redundant computation, and lack of cross-variable interaction. Our study addresses these limitations by proposing a multi-task, multi-variable Vision Transformer (ViT) architecture with a shared encoder and variable-specific decoders (1EMD). The proposed architecture jointly predicts three key climate variables: surface temperature (tas), wind speed (sfcWind), and 500 hPa geopotential height (zg500), directly from GCM-resolution inputs, emulating RCM-scale downscaling over Europe. We show that our multi-variable approach achieves positive cross-variable knowledge transfer and consistently outperforms single-variable baselines trained under identical conditions, while also improving computational efficiency. These results demonstrate the effectiveness of multi-variable modeling for high-resolution climate downscaling.

**keywords:** climate downscaling, climate model emulation, vision transformers, multi-task learning, multi-variable models

## 1 Introduction

Global Climate Models (GCMs) are essential tools for simulating the Earth’s climate system and projecting future climate change. However, their coarse spatial resolution, typically around  $1^\circ$ , limits their ability to accurately capture regional-scale dynamics. To overcome this limitation, Regional Climate Models (RCMs) are employed to dynamically downscale GCM outputs, providing finer-scale climate information at resolutions typically ranging from 10 to 50 kilometers. Although RCMs enhance spatial detail and realism, they are computationally demanding, limiting the number of possible model runs in the context of regional coordinated experiments [1].

An emerging alternative to traditional numerical downscaling involves the use of deep learning techniques to emulate the RCM downscaling process. Instead of performing computationally intensive simulations, deep learning models learn to reproduce the mapping from coarse-resolution GCM outputs to high-resolution RCM fields from available data. This approach presents a rapid, data-driven method for producing detailed climate projections applicable across multiple regions and scenarios, increasing the number of available simulations [2].

In this study, we frame the GCM-to-RCM emulation task as a supervised deep learning problem. Using paired datasets from GCM and RCM outputs, we employ Vision Transformer (ViT) models to learn the relationship between coarse-resolution inputs and their high-resolution counterparts over the European domain. The primary objective of this approach is to produce spatially detailed outputs that accurately capture the fine-scale structures inherent to RCM simulations, enabling efficient and cost-effective generation of high-resolution climate data.

The main contribution of this work is the exploration of joint, multi-variable processing. Typically, downscaling meteorological variables from GCM to RCM involves handling numerous diverse variables spanning atmospheric, surface, and radiation categories. Most existing deep learning approaches for climate downscaling focus exclusively on single-variable modeling, training and applying uni-variate models separately on each variable [3–7]. This approach poses several issues: single-variable models cannot exploit valuable cross-variable interactions, managing and executing multiple independent models is inefficient, and similar meteorological variables result in redundant learning efforts when modeled separately. In response, this study explores multi-variable processing strategies.

Vision Transformers (ViTs) have emerged as powerful architectures in image-to-image translation and super-resolution tasks due to their attention-based processing and ability to capture long-range dependencies [2, 8–10]. Leveraging this architecture, we propose processing several meteorological variables simultaneously, enabling the effective exploitation of inter-variable relationships and potentially enhancing overall performance and physical coherence. This approach significantly reduces the number of required models, thereby decreasing computational demands per variable and improving efficiency. However, multi-variable modeling also introduces challenges such

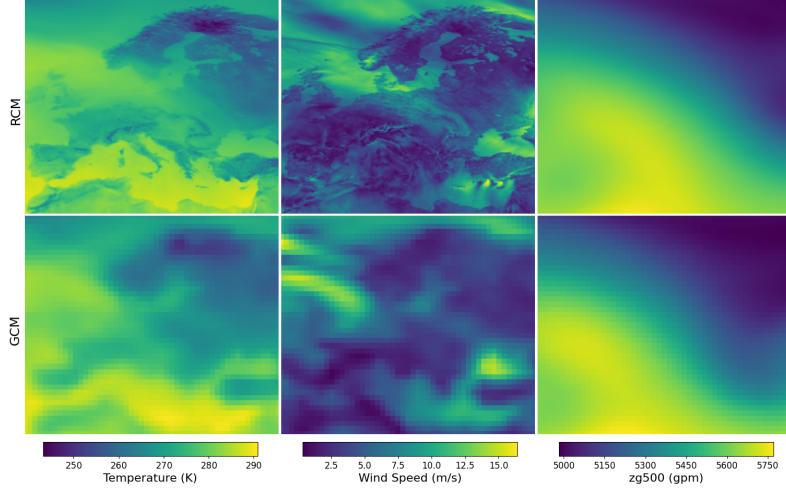


**Fig. 1:** Visualization of a single daily sample for the three studied variables: surface temperature (left column), wind speed (center column), and geopotential height (right column). Each variable is shown for both the high-resolution Regional Climate Model ICTP-RegCM4-6 (top row) and the low-resolution Global Climate Model MPI-ESM-LR (bottom row) re-gridded onto the same European domain.

as potential training instabilities and cross-variable interference, which may manifest as artifacts in outputs.

To evaluate multi-variable modeling strategies for GCM-to-RCM downscaling, we leverage modern ViT architectures to model this image-to-image translation problem. Our study focuses on three common meteorological variables: wind speed (sfcWind), temperature (tas), and geopotential height at 500 hPa (zg500). An image depicting a sample of the three variables for both RCM and GCM is reported in Figure 1. We first establish baseline performance using single-variable ViT models trained independently for each variable. Subsequently, we introduce two multi-variable approaches: one treating variables as separate channels (1E1D), and a second employing a single shared encoder with multiple dedicated decoders (1EMD), one per variable. We ensure a robust and reproducible comparison by standardizing model structure, parameter count, training epochs, learning rates, and optimizers across all experiments.

Our findings reveals that multi-variable modeling offers clear advantages in terms of computational efficiency. However, the simpler multi-channel approach (1E1D) suffers from cross-variable interference, failing to match the performance of single-variable baselines. In contrast, our structured multi-decoder design (1EMD) avoids these issues and outperforms single-variable models across all tested variables. These results highlight the effectiveness of our multi-variable architecture for high-resolution climate downscaling.

## 1.1 Data Selection

Our study is based on the EURO-CORDEX data. EURO-CORDEX, developed as part of the Coordinated Regional Downscaling Experiment (CORDEX) under the World Climate Research Programme (WCRP), provides a consistent set of high-resolution ( $0.11^\circ$ ) RCM simulations, driven by boundary conditions from multiple GCMs and emission scenarios. These simulations are widely used for regional climate impact assessments across Europe [1]. We subjectively selected one GCM-RCM couple from the available simulations: the MPI-ESM-LR GCM with the ICTP-RegCM4-6 RCM simulation under emissions scenario RCP8.5.

The selection of surface air temperature (tas), surface wind speed (sfcWind), and geopotential height at 500 hPa (zg500) was guided by a combination of practical relevance and methodological interest. The three variables exhibit markedly different spatial characteristics when downscaled. Surface temperature tends to produce relatively smooth spatial fields varying mostly with elevation and latitude, surface wind speed fields often feature localized and high-frequency patterns, and geopotential height exhibits broad, smooth spatial gradients that reflect the large-scale atmospheric circulation patterns in the mid-troposphere. This diversity offers a useful testbed for evaluating how well data-driven models handle different signal types, and whether modeling them jointly can facilitate positive transfer across variables.

The choice was also shaped by the broader goal of exploring multi-variable downscaling. By selecting a small but diverse set of variables, we can begin to assess whether downscaling performance benefits from shared representations across related but physically distinct fields. The downscaling task addresses a spatial resolution increase from  $1.0^\circ$  to  $0.1^\circ$ , representing a tenfold enhancement. This is among the largest resolution gaps available in publicly accessible GCM-RCM datasets, offering a particularly demanding test case for evaluating the capabilities of data-driven downscaling methods.

The domain of interest is Europe, selected for its climatic diversity, data availability, and relevance to policy and research communities. To ensure a direct comparison between scales, the low-resolution GCM data was interpolated onto the RCM's  $0.1^\circ$  grid using bilinear interpolation. This pre-processing step ensures that GCM and RCM fields are directly comparable in both space and time. The datasets span daily time steps from 2006 to 2099.

## 1.2 Related Works

In recent years, the focus of climate downscaling has increasingly shifted toward deep learning models [3, 11, 12]. A wide range of architectures has been explored to downscale variables such as temperature, wind components, surface pressure, and precipitation, among others. These include convolutional neural networks (CNNs) [4, 12–16], U-Nets [6, 17, 18], Vision Transformers (ViTs) [8–10], generative adversarial networks (GANs) [19–22], and diffusion models [23–27].

Different architectures show varying strengths depending on the target variable. Generative models like GANs and diffusion models are particularly effective at preserving high-frequency spatial detail and have shown strong performance in downscaling



wind speed [28]. In contrast, smoother fields such as temperature are often better handled by U-Nets [29]. Despite these findings, there is no clear consensus on a universally optimal architecture. Recently, ViT-based models have shown competitive and often superior performance across multiple climate variables, outperforming CNN-based baselines in several studies [8, 30, 31]. As such, ViTs form the foundation of our proposed approach.

ViT-based architectures for image-to-image tasks often draw inspiration from the encoder-decoder structure of U-Nets. One common design integrates a transformer-based encoder with a convolutional decoder [32–34], while other variants opt for fully transformer-based pipelines [35, 36]. A key architectural consideration is the treatment of skip connections, which preserve spatial resolution and improve gradient flow. These may be preserved directly [32, 37], omitted entirely under the assumption of rich encoder representations [33], or implemented through attention-based gating mechanisms [35].

While the majority of deep learning-based downscaling studies employ single-variable models, where each variable is modeled independently, there is growing interest in multi-variable approaches that leverage cross-variable relationships. These approaches aim to enhance physical consistency across variables and potentially improve accuracy. In this work, we design a multi-variable downscaling framework and benchmark its performance against single-variable counterparts.

Multi-variable downscaling naturally aligns with the framework of multi-task learning, where a single model learns to solve multiple related tasks simultaneously. In climate applications, multi-task learning offers several potential advantages: improved generalization through shared representations, reduced training and inference cost, and the possibility of positive transfer across variables [38].

Several recent studies support the promise of this approach. For instance, Ling et al. [39] present a multi-task model for seasonal climate prediction that jointly forecasts several indices related to the Indian Ocean Dipole. The model is trained using a loss function defined as a weighted sum of the individual task with a higher loss weight to the primary target (DMI). The model achieves improved performance compared to single-variable baselines. Similarly, Fan et al. [40] propose M2GSNet, a graph-based multi-task model for wind power prediction across multiple farms. By utilizing shared encoders across tasks and training with an unweighted sum of L1 losses across farms, the model achieves superior forecasting accuracy compared to single-variable baselines.

Other examples further support the benefits of multi-task formulations. Bannai et al. [41] use a shared CNN backbone with two heads for simultaneous rain/no-rain classification and rain rate estimation, yielding improved performance through joint optimization of a combined loss function. Liu et al. [42] propose a two-stage downscaling system incorporating bias correction, terrain inputs, and a multi-task loss with physical constraints, demonstrating the potential of multi-variable models for enhancing both accuracy and realism in climate data products.

## 2 Methodology

In this section, we start by detailing our backbone implementation of a ViT-based image-to-image model. We then proceed to describe the single-variable approach, where separate encoder-decoder architectures are trained independently for each target variable. Next, introduce two multi-variable strategies. The first, a single-encoder single-decoder (1E1D) model, concatenates multiple variables along the channel dimension, treating them as multi-channel images in a unified ViT pipeline, and the second a single-encoder multi-decoder (1EMD) where a shared encoder extracts common features, while separate decoders are dedicated to reconstructing each variable individually. A visual comparison of the proposed approaches is shown in Figure 2.

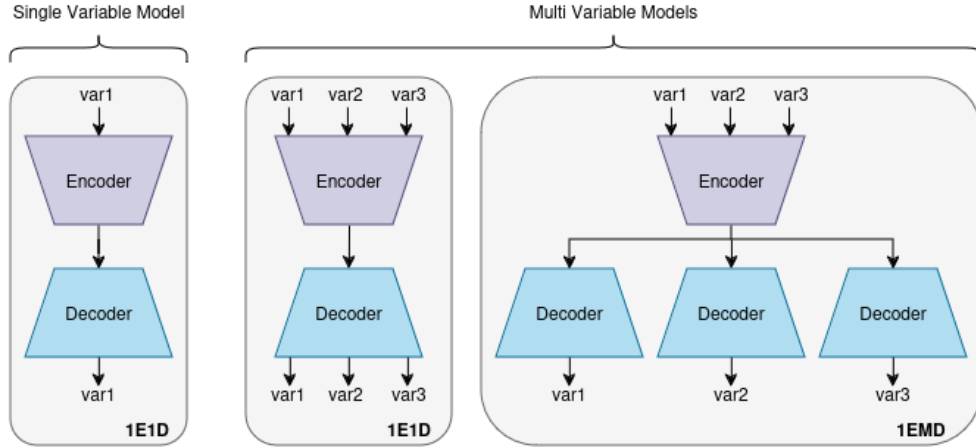


**Fig. 2:** Comparison between a single-variable encoder-decoder model and multi-variable models using either a single shared decoder (1E1D) or multiple decoders branching from a shared encoder (1EMD)

### 2.1 Architectural Backbone: Vision Transformer (ViT)

Vision Transformers (ViTs) are neural architectures that originate in natural language processing, where self-attention is used to capture relationships within sequences. In the vision domain, ViT applies the same principle by splitting an image into fixed-size patches, which are then flattened, embedded, and treated as a sequence. This sequence is processed by transformer blocks, allowing the model to capture global image dependencies without relying on convolutions, effectively serving as an alternative to traditional encoder networks.

In recent years ViTs have been successfully applied to a variety of super-resolution tasks [43–46]. Our proposed ViT architecture belongs to the ViT-CNN hybrid category, combining a transformer-based encoder with a convolutional decoder, enabling

the model to capture global, non-local relationships more effectively than purely convolutional networks [32, 34]. This design allows the model to handle complex spatial patterns, which is especially important for tasks that require modeling long-range and cross variable dependencies.

Skip connections are a well-established component of encoder-decoder architectures, commonly used to preserve spatial detail and improve gradient flow. In ViT-CNN hybrid models, studies have shown that skip connections can enhance performance by bridging lower-level features from the encoder to the decoder [32]. However, in transformer-based architectures, especially those without hierarchical designs, this benefit may be less critical [33, 47]. Unlike CNN encoders, which typically reduce spatial resolution through downsampling, our ViT encoder preserves a constant resolution throughout. As a result, the output tokens retain the same spatial structure as the input, reducing the need for skip connections to recover lost detail.

In our implementation, we chose to omit skip connections to prioritize modularity and simplicity, particularly in the context of supporting multiple variable-specific decoders. In a multi-decoder setting, implementing skip connections would require duplicating and routing encoder features to each decoder, increasing architectural complexity and coupling. Moreover, since each decoder specializes in a different output variable, sharing low-level features indiscriminately across all decoders could introduce unintended interactions or noise between tasks, potentially harming performance. Given that the empirical benefits of skip connections in transformer encoders remain inconclusive, we deemed the flexibility of a skip-free design—enabling easy addition or removal of decoders—more valuable than a potentially marginal performance gain.

Specifically, our architecture is designed as follows: The encoding path follows a standard ViT configuration, where the input image is divided into non-overlapping  $8 \times 8$  patches, each linearly projected into a 256-dimensional vector by a dense embedding layer. To retain spatial information, learnable positional embeddings are added to the patch representations before passing them through the transformer stack. The encoder consists of six transformer layers, each following a consistent structure. Each layer applies normalization, followed by multi-head self-attention with eight heads and a dropout rate of 0.1. Next, A residual connection adds the input of the attention block to its output. After attention, a second normalization is applied, followed by a multi-layer perceptron (MLP) consisting of two fully connected layers with 512 and 256 units, respectively, and GELU [48] activation. Another residual connection is applied at the output of the MLP block. Through this process, the transformer encoder learns both local and global relationships between spatially distributed patches. To mitigate the memory constraints that limit batch size, we use Group Normalization [49] with a group size of 8, which has been shown to be more stable than Batch Normalization in such settings.

Following the transformer encoder, the sequence of embeddings is reshaped into a spatial grid, initializing the decoding path. The decoder is composed of three consecutive upsampling blocks, each of which includes bilinear interpolation for upsampling, doubling the spatial resolution at each step. We utilize bilinear interpolation avoiding artifacts often associated with learned transposed convolutions [50]. Each bilinear upsampling is followed by a residual block, composed of group normalization, two

convolutional layers, and a residual connection that preserves input information. The first convolution in the block uses Swish activation, while the second uses no activation. The feature width begins at 256 in the first upsampling block and is halved in each subsequent block, reducing to 32 in the final block. A final convolutional layer with no activation and a kernel initializer set to zero projects the output to the target resolution, completing the decoding process. The complete architecture for a single encoder-decoder pair contains approximately 11 million learnable parameters.

## 2.2 Single-Variable Models

The most direct approach at downscaling multiple variables is based on the use of multiple single-variable models trained independently on each variable, with no sharing of weights or other information between each model.

Each individual model consists of a single encoder-decoder pair, which enables the model to focus on the individual task but doesn't enable the utilization of cross-variable information.

In the case of single variable the loss is calculated on the comparison between the generated output and the available ground truth, with our implementation using mean square error (MSE) loss. Denoting  $\hat{Y}_{hw}$  as the predicted pixel at spatial position  $(h, w)$  and  $Y_{hw}$  as the corresponding ground truth pixel, the loss is defined as:

$$\mathcal{L}_{\text{MSE}} = \frac{1}{HW} \sum_{h=1}^H \sum_{w=1}^W \left( \hat{Y}_{hw} - Y_{hw} \right)^2 \quad (1)$$

## 2.3 Multi-Variable Models

The main goal of this work is to design an architecture capable of downscaling multiple variables simultaneously. While the coarse-resolution GCM provides the primary input, we hypothesize that additional value can be gained by exploiting inter-variable relationships. Our assumption is that the atmospheric state encodes joint spatial and dynamical patterns across variables, which a shared representation can capture more effectively than isolated models. By modeling all variables together, the network can leverage these patterns, potentially leading to improved accuracy and greater physical consistency compared to independent downscaling approaches.

Building upon the ViT architecture described in Section 2.1, we implement two multi-variable variants: a Single-Encoder Single-Decoder (1E1D) model, where all variables share the same encoder-decoder pipeline, and a Single-Encoder Multi-Decoder (1EMD) model, where the variable are jointly encoded but decoded separately. These designs allows us to study the trade-off between fully shared architectures and variable-specific specialization via independent decoders.

Both our proposed multi-variable approaches share the same loss structure. Training is performed simultaneously across the three target variables, with the loss computed as the mean over all output channels. To make this approach viable, it is essential to normalize all variables to the same range. This ensures that the model optimizes all variables with equal priority, preventing any one variable from dominating the loss due to scale differences. With MSE being our loss function of choice, and

denoting  $\hat{Y}_{nhw}$  as the predicted pixel at spatial position  $(h, w)$  for variable  $n$ , and  $Y_{nhw}$  as the corresponding ground truth pixel, the joint loss is defined as:

$$\mathcal{L}_{\text{MSE}} = \frac{1}{NHW} \sum_{n=1}^N \sum_{h=1}^H \sum_{w=1}^W \left( \hat{Y}_{nhw} - Y_{nhw} \right)^2 \quad (2)$$

### 2.3.1 Single-Encoder Single-Decoder VIT (1E1D)

Our first approach to multi-variable modeling treats the different atmospheric fields as complementary features of a single spatial input by concatenating the variables along the channel dimension. This design keeps the single-variable architecture largely intact, with modifications only to the patch embedding and final convolutional layers to accommodate three input and output channels.

The input consists of three geophysical variables stacked as a three-channel image. We divide this input into non-overlapping patches of shape  $8 \times 8 \times 3$ , each of which is projected into a 256-dimensional vector via a dense embedding layer. These token embeddings are then processed by a Vision Transformer (ViT) encoder, following the same architecture used in the single-variable model. The decoder, composed of convolutional layers, upsamples the latent representation back to the original spatial resolution, with the final layer producing three output channels corresponding to the predicted fields.

This approach allows the encoder to capture a joint representation of the atmospheric state across multiple variables. However, it implicitly assumes that the variables are spatially aligned and semantically compatible when treated as separate channels, an assumption that may be limiting if the variables exhibit different spatial structures or temporal dynamics.

### 2.3.2 Single-Encoder Multi-Decoder VIT (1EMD)

The three target variables in our downscaling task exhibit substantial differences in their spatial structures and statistical distributions. For example, temperature fields tend to show smoother gradients compared to the more intricate patterns found in wind components. When using a single decoder to reconstruct all variables jointly, these differences can cause interference: the decoder is limited to sharing the same weights for generating the different variables, leading to potential cross-variable contamination. In particular, we observed that high-frequency patterns from one variable (e.g., wind) can bleed into the smoother reconstructions of another (e.g., geopotential height), degrading performance.

To address this, we propose a novel multi-variable downscaling architecture that employs a single transformer-based encoder shared across all variables, followed by a dedicated convolutional decoder for each output variable. This design preserves the benefit of jointly encoding spatial inter-variable dependencies while allowing each decoder to specialize in reconstructing a specific variable. By decoupling the decoding paths, we reduce interference and provide sufficient representational capacity to each output stream. We consider this architecture to be an effective compromise between

the two aforementioned approaches: running completely independent encoder-decoder pipelines for each variable, and forcing all variables through a single encoder-decoder with channel concatenation. Our approach leverages shared context while controlling model complexity and avoiding cross-variable entanglement, achieving a favorable trade-off between accuracy and computational cost.

Specifically, the 1EMD architecture is structured as follows. Each low-resolution input variable is first bilinearly upsampled to the target resolution of  $504 \times 432$ , matching the output grid. The resulting variables are concatenated along the channel dimension and partitioned into 3402 non-overlapping patches of size  $8 \times 8 \times 3$ . Each patch is linearly embedded into a 256-dimensional vector and augmented with positional information via additive encoding. The sequence of embedded patches is processed by a stack of six transformer blocks, each featuring multi-head self-attention (six heads), residual connections with group normalization, and MLP layers with GELU activations.

The final encoder output is reshaped into a spatial feature grid of size  $54 \times 63 \times 256$  and passed in parallel to three independent convolutional decoders, one per variable. The decoders do not share parameters and are trained jointly using a composite loss function that accounts for all variables. Each decoder consists of a sequence of residual blocks with group normalization and Swish activations, interleaved with 2D upsampling layers. Three upsampling stages are used to restore the original resolution of  $504 \times 432$ . The final output is produced by a zero-initialized convolutional layer without activation. The complete 1EMD model architecture is reported in Figure 3.

Experimental results, discussed in detail in Section 4, demonstrate that the proposed 1EMD model outperforms both the single-variable and 1E1D approaches.

### 3 Experimental Setup

Our objective is to learn a mapping from coarse-resolution Global Climate Model (GCM) to high-resolution Regional Climate Model (RCM). Specifically, we use data from the MPI-ESM-LR GCM and the ICTP-RegCM4-6 RCM under the RCP8.5 scenario, addressing a spatial resolution shift from  $1^\circ$  (approximately 100 km) to  $0.1^\circ$  (approximately 10 km). The GCM data are re-gridded to the RCM domain using bilinear interpolation to match the spatial structure of the RCM over Europe.

We focus on downscaling three key atmospheric variables: near-surface air temperature (tas), surface wind speed (sfcWind), and 500 hPa geopotential height (zg500). From an image processing perspective, each variable is treated as a 2D field with spatial dimensions of  $431 \times 501$  pixels.

Our dataset spans daily values from 2006 to 2100. We use data from 2006–2099 for training and reserve one year per decade (2010, 2020, etc.) for testing. This design avoids long-term temporal separation between training and test sets, helping prevent bias from trends such as climate change. For each variable, GCM and RCM outputs are temporally and spatially aligned so that the models can effectively learn to predict high-resolution RCM fields from corresponding low-resolution GCM inputs.

As of pre-processing, each variable is min-max normalized to the  $[0, 1]$  range using the training data’s minimum and maximum values. To ensure compatibility

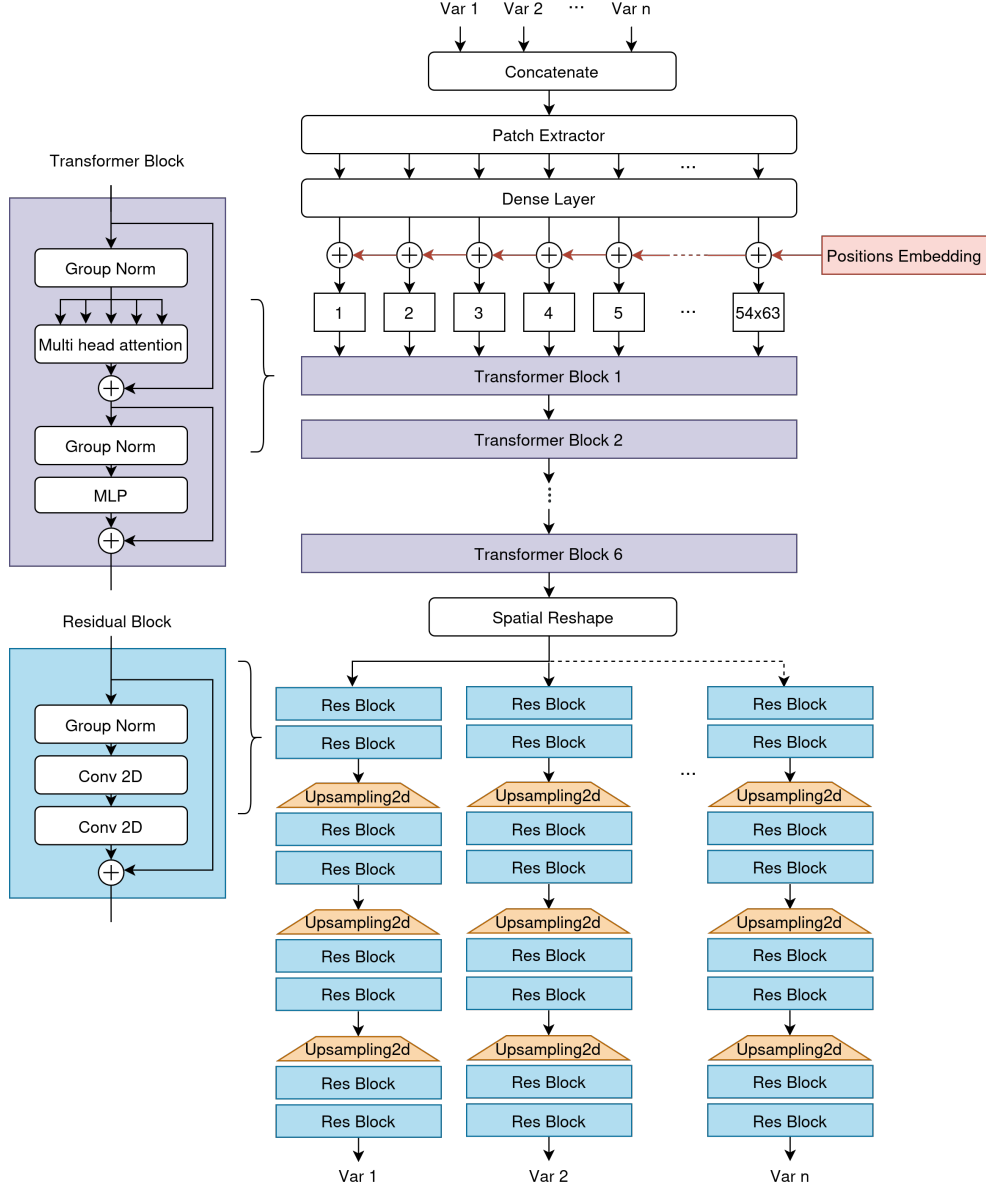


**Fig. 3:** Architecture of the multi-variable single-encoder multi-decoder model (1EMD). Concatenated input variables are divided into patches, embedded with positional encodings, and processed as a sequence by six transformer blocks, each consisting of multi-head self-attention (6 heads) followed by an MLP. The output sequence is then reshaped into a spatial grid and passed to separate CNN-based decoders, each composed of three upsampling stages interleaved with residual blocks.



with convolutional architectures, images are also padded via replication to  $432 \times 504$  pixels to make the dimensions divisible by 8. Padding is removed before computing evaluation metrics.

Our downscaling models operate in an image-to-image manner, taking the GCM variable(s) at a given timestamp as input and predicting the corresponding RCM variable(s). In the single-variable case, the model maps one GCM field to one RCM field. In the multi-variable case, the model maps all three GCM variables to their corresponding RCM fields for the same timestamp, effectively forming a three-to-three mapping as illustrated in Figure 2.

We adopt a fair comparison framework that is coherent with standard practice in model comparison, avoiding common pitfalls such as unequal fine-tuning, training effort or model complexity [51–53]. We compare three modeling approaches, all based on a Vision Transformer (ViT) backbone. First, we train individual single-variable models for each of the three variables. Then, we explore two multi-variable models: 1E1D, which uses a shared encoder and decoder, and 1EMD, which employs a shared encoder and separate decoders for each variable.

All models share the same encoder architecture. The single-variable ViT and the multi-variable ViT 1E1D also share the same parameter count, differing only in the final convolutional layer and decoder embeddings. In contrast, the 1EMD model maintains a shared encoder but uses three independent decoders (one per variable), with no weight sharing in the decoding stage.

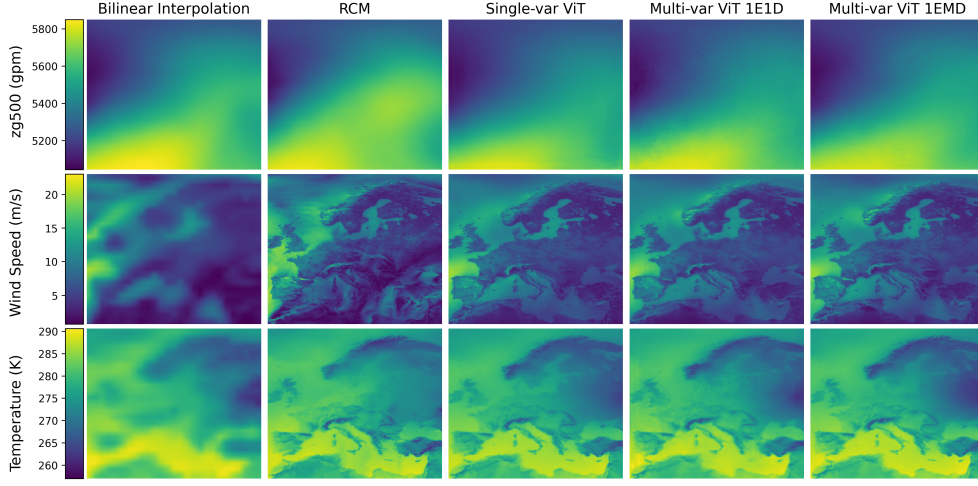
We use the Adam optimizer with decoupled weight decay (AdamW) [54], a common choice for ViT-based architectures. All models are trained for 400 epochs with 500 steps per epoch. Due to memory constraints, we use a batch size of 1. The learning rate is fixed at  $1e-4$  for the first 300 epochs and reduced to  $1e-5$  for the final 100 epochs. Weight decay is set to one-tenth of the current learning rate. These settings were chosen based on empirical tuning to ensure consistent convergence across all approaches. We use mean squared error (MSE) as the loss function for all models, as described in Sections 2.2 and 2.3.

Training is conducted on a NVIDIA A100 GPU using a unified pre-processing pipeline. Testing is performed on the reserved ten years of test data, spanning the full 100-year period. Each model is evaluated on the entire test set, and performance metrics are computed over all test samples.

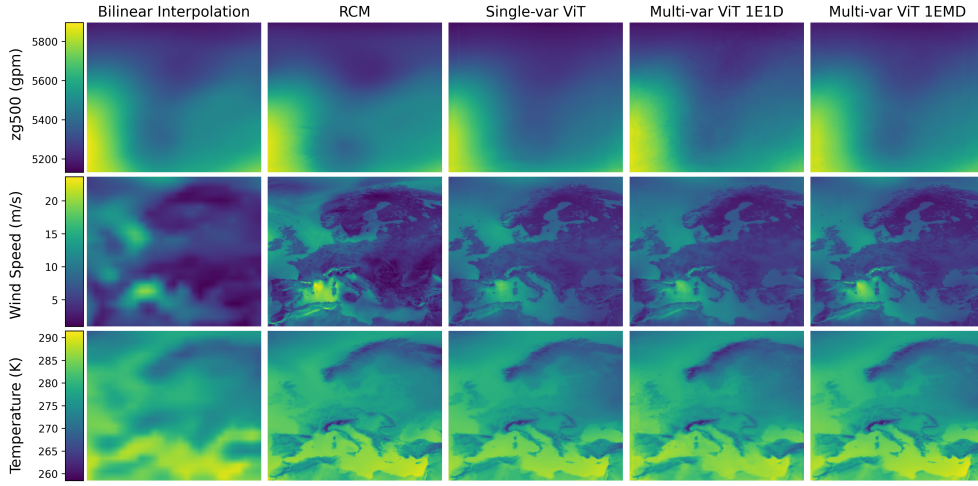
## 4 Results

We evaluate the three models, Single-variable ViT, Multi-variable ViT (1E1D), and Multi-variable ViT (1EMD) on a test dataset comprising ten years of unseen data. The test set includes one year per decade from 2010 to 2100.

All models are tested across the three selected variables: surface temperature (tas), wind speed (sfcWind), and 500 hPa geopotential height (zg500), using three evaluation metrics: Mean Squared Error (MSE), Mean Absolute Error (MAE), and Structural Similarity Index (SSIM). These metrics offer a well-rounded perspective, balancing numerical accuracy (MSE, MAE) with perceptual similarity (SSIM), and are commonly adopted in climate imaging studies [3, 5, 55–57].



(a)



(b)

**Fig. 4:** Comparison of the examined models (Single var ViT, multi var ViT 1E1D, Multi var ViT 1EMD), target RCM, and bilinearly interpolated GCM for two different samples of the test set. For each sample, each row contains geopotential, wind speed and temperature for the same timestamp.

All metrics are computed on normalized data to enable cross-variable comparison as the variables differ in their units and ranges.

GCM to RCM Downscaling Performance (MPI to RegCM)			
Model	MSE ↓	MAE ↓	SSIM ↑
<b>tas</b>			
Bilinear	3.31e-03	4.82e-02	9.69e-01
Single Var. ViT	4.37e-04	1.47e-02	<u>9.88e-01</u>
Multi Var. ViT (1E1D)	4.63e-04	1.52e-02	9.84e-01
Multi Var. ViT (1EMD)	<u>4.19e-04</u>	<u>1.43e-02</u>	<u>9.88e-01</u>
<b>sfcWind</b>			
Bilinear	7.22e-03	6.40e-02	8.05e-01
Single Var. ViT	3.45e-03	4.37e-02	8.82e-01
Multi Var. ViT (1E1D)	3.31e-03	4.26e-02	8.79e-01
Multi Var. ViT (1EMD)	<u>3.24e-03</u>	<u>4.21e-02</u>	<u>8.87e-01</u>
<b>zg500</b>			
Bilinear	2.55e-03	3.76e-02	<u>9.95e-01</u>
Single Var. ViT	1.89e-03	3.17e-02	<u>9.95e-01</u>
Multi Var. ViT (1E1D)	1.88e-03	3.15e-02	9.94e-01
Multi Var. ViT (1EMD)	<u>1.81e-03</u>	<u>3.10e-02</u>	<u>9.95e-01</u>

**Table 1:** Model performance comparison for downscaling from MPI-ESM-LR to RegCM4-6 for each variable. Best values for each variable are underlined, the results are computed for variables normalized between 0 and 1. Best results (including ties) are underlined.

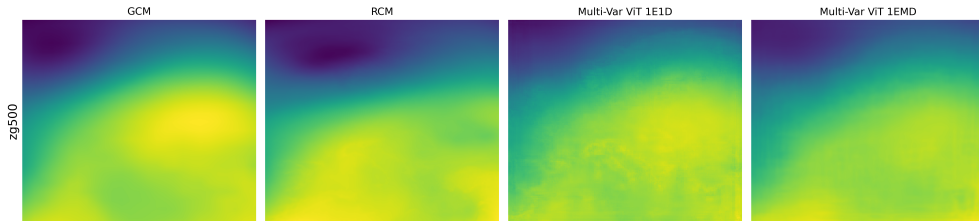


**Fig. 5:** Visualization of cross-variable leakage in the 1E1D model for zg500. From left to right: original GCM input, target RCM output, prediction from the 1E1D model, and prediction from the 1EMD model. While zg500 is expected to be spatially smooth, the 1E1D prediction exhibits faint outlines resembling European geography, suggesting contamination from temperature and wind fields. This artifact is absent in the 1EMD model, which treats each variable with dedicated decoder pathways.

Table 1 reports the numerical results for all models and variables. We also include bilinear interpolation as a baseline, applied directly to the GCM data before comparison with RCM targets. Figure 4 provides a visual comparison of all models alongside the original RCM data for two randomly selected test samples.

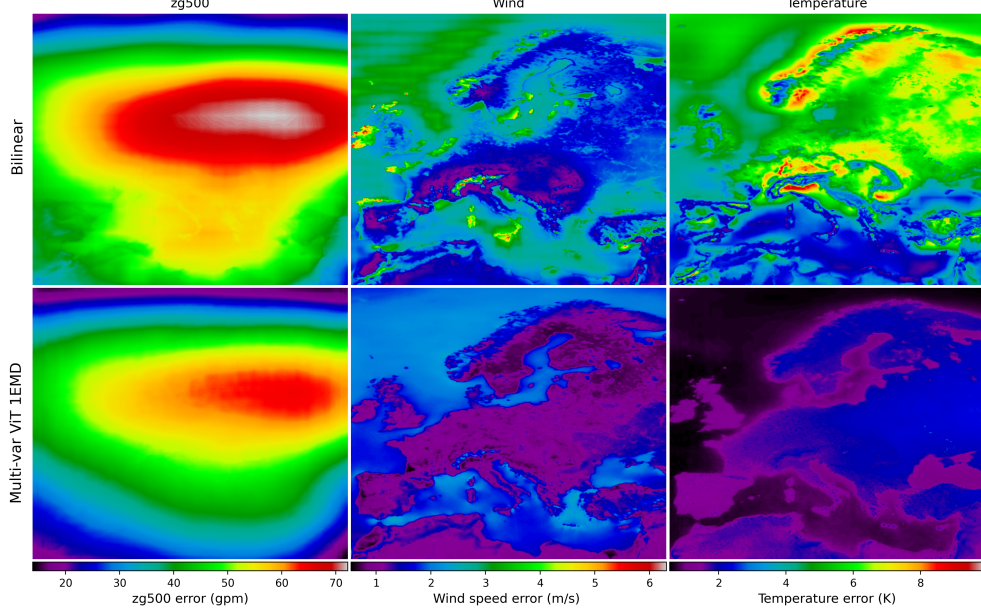


**Fig. 6:** Mean absolute error maps comparing the performance of bilinear interpolation (top row) and the multi-variable, multi-decoder 1EMD ViT model (bottom row). Each column shows the spatial distribution of errors for one variable: geopotential height at 500 hPa (zg500), 10-meter wind speed, and near-surface temperature. The error are computed for the complete test set, color bars are individually scaled per variable

The Single-variable ViT consistently improves upon the bilinear interpolation baseline across all three variables. In the case of surface temperature (tas), the Single-variable ViT reduces MSE from  $3.31\text{e-}03$  to  $4.37\text{e-}04$ , and improves SSIM from 0.969 to 0.988. Similar improvements are observed for wind speed, where the MSE drops from  $7.22\text{e-}03$  to  $3.45\text{e-}03$ , and for zg500, where it decreases from  $2.55\text{e-}03$  to  $1.89\text{e-}03$ .

The Multi-variable ViT (1E1D) model improves over the Single-variable ViT for wind speed but performs worse on temperature and geopotential. This suggests that a single decoder doesn't have sufficient capacity to model the three distinct variables simultaneously. The observed performance degradation indicates that the shared decoder architecture is likely a limiting factor, as it cannot fully exploit cross-variable information without compromising variable-specific accuracy. Additionally, the 1E1D model exhibits cross-variable leakage in zg500, with geographic artifacts emerging in the output, as illustrated in Figure 5.

The Multi-variable ViT (1EMD) achieves the best results across all variables. Compared to the Single-variable ViT, For tas, MSE decreases from  $4.37\text{e-}04$  to  $4.19\text{e-}04$  while SSIM remains at 0.988. For wind speed, the MSE is further reduced from  $3.45\text{e-}03$  to  $3.24\text{e-}03$  and SSIM increases from 0.882 to 0.887. For zg500, MSE drops from  $1.89\text{e-}03$  to  $1.81\text{e-}03$ . These results indicate that, under fair training conditions, a multi-task design with dedicated decoders is capable of leveraging cross-variable

relationships to improve overall performance. To further assess the performance of 1EMD, a visual comparison of mean absolute error maps between 1EMD and bilinear interpolation is reported in Figure 6.

Multi-variable models offer clear efficiency advantages by consolidating multiple downscaling tasks into a single model, utilizing a single shared encoder thus reducing the number of computations and requiring fewer model initializations overall. To quantify this, we measure the inference time for each model to generate predictions over the 10-year test dataset. All models are run on the same hardware and share a unified pre-processing pipeline.

Figure 7 presents the total runtime per model (in seconds), along with per-variable time for multi-variable models which process all three variables simultaneously.

The results show that, on a per-variable basis, the multi-variable models achieve approximately 25% faster inference compared to equivalent single-variable models.

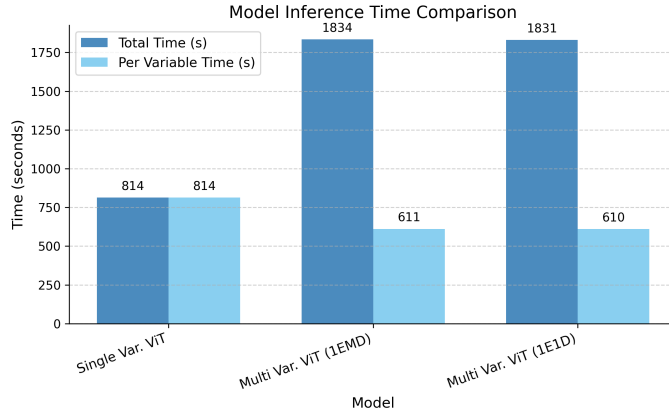


**Fig. 7:** Inference time comparison across model architectures. The Total inference time (dark blue bars) and per-variable inference time (light blue bars) are shown for three model configurations. All models were evaluated on identical hardware (NVIDIA A100), with batch size 1 and the same input data pipeline. The measurements correspond to the inference time required to process 10 years of daily testing data (3650 samples). For the multi-variable models, which predict three variables simultaneously, the per-variable inference time was calculated by dividing the total inference time by three.

## 5 Conclusion

In this study, we have explored multi-variable deep learning approaches for climate downscaling, specifically targeting the GCM-to-RCM emulation task. While most deep learning approaches focus on modeling single variables, we have argued that jointly processing multiple variables can improve both efficiency and predictive performance.

Redundant modeling across variables can be avoided, and information from one variable can enhance the prediction of another by capturing inter-variable dependencies. To test this hypothesis, we designed three model configurations using a shared Vision Transformer (ViT)-based encoder-decoder architecture. These configurations explore different strategies for handling multiple variables, ranging from fully independent models to joint encoding with separate decoders. This progression allowed us to assess the trade-offs between variable separation and shared representation, culminating in our proposed Multi Var. ViT (1EMD) model, which combines a shared encoder with dedicated decoders for each variable. To rigorously evaluate our methods, we established a consistent and fair comparison framework. All models share the same architecture, differing only in the components necessary to support multi-variable processing. Training hyperparameters, learning rate scheduling, pre-processing pipelines, and hardware resources were kept identical across all experiments. Our results, based on a 10-year test set of held-out data, demonstrate that the proposed Multi Var. ViT (1EMD) model consistently outperforms all other tested configurations. This suggests that combining shared representations with variable-specific decoders is an effective strategy for multi-variable downscaling. Overall, we have introduced an effective and straightforward method for climate downscaling in a multi-variable context. By modeling variables jointly, our results suggest a substantial gain in both performance and computational efficiency. Several open questions remain, including how many variables can be effectively modeled together, which variables should be selected to maximize performance, and whether more sophisticated loss functions could further enhance the model’s capabilities.

## Declarations

### Funding

This research was partially funded and supported by the following Projects:

- European Cordis Project “Optimal High Resolution Earth System Models for Exploring Future Climate Changes” (OptimESM), Grant agreement ID: 101081193
- ISCRA Project “AI for weather analysis and forecast” (AIWAF)

### Acknowledgements

We are grateful to Thomas Noël (TCDF) for providing access to the GCM–RCM simulation data used in this study. We also thank Leone Cavicchia and Enrico Scoci-marro (CMCC) for their valuable insights and constructive discussions, which helped improve the quality of this work.

### Statements

The authors declare no competing interests.

## Code and data availability

The code is available from the authors upon reasonable request.

The data used in this study were obtained from the CORDEX archive hosted on the Earth System Grid Federation (ESGF) via the IPSL node <https://esgf-node.ipsl.upmc.fr/search/cordex-ipsl/>

## References

- [1] Daniela Jacob, Juliane Petersen, Bastian Eggert, Antoinette Alias, Ole Bøssing Christensen, Laurens M. Bouwer, Alain Braun, Augustin Colette, Michel Déqué, Goran Georgievski, Elena Georgopoulou, Andreas Gobiet, Laurent Menut, Grigory Nikulin, Andreas Haensler, Nils Hempelmann, Colin Jones, Klaus Keuler, Sari Kovats, Nico Kröner, Sven Kotlarski, Arne Kriegsmann, Eric Martin, Erik van Meijgaard, Christopher Moseley, Susanne Pfeifer, Swantje Preuschmann, Christine Radermacher, Kai Radtke, Diana Rechid, Mark Rounsevell, Patrick Samuelsson, Samuel Somot, Jean-Francois Soussana, Claas Teichmann, Riccardo Valentini, Robert Vautard, Björn Weber, and Pascal Yiou. Euro-cordex: new high-resolution climate change projections for european impact research. *Regional Environmental Change*, 14(2):563–578, Apr 2014.
- [2] Neelesh Rampal, Sanaa Hobeichi, Peter B. Gibson, Jorge Baño-Medina, Gab Abramowitz, Tom Beucler, Jose González-Abad, William Chapman, Paula Harder, and José Manuel Gutiérrez. Enhancing regional climate downscaling through advances in machine learning. *Artificial Intelligence for the Earth Systems*, 3, 3 2024.
- [3] Jorge Baño-Medina, Rodrigo Manzananas, and José Manuel Gutiérrez. Configuration and intercomparison of deep learning neural models for statistical downscaling. *Geoscientific Model Development*, 13(4):2109–2124, 2020.
- [4] Thomas Vandal, Evan Kodra, Sangram Ganguly, Andrew Michaelis, Ramakrishna Nemani, and Auroop R Ganguly. DeepSD: Generating high resolution climate change projections through single image super-resolution. In *Proceedings of the 23rd acm sigkdd international conference on knowledge discovery and data mining*, pages 1663–1672, 2017.
- [5] Norihiro Oyama, Noriko N Ishizaki, Satoshi Koide, and Hiroaki Yoshida. Deep generative model super-resolves spatially correlated multiregional climate data. *Scientific Reports*, 13(1):5992, 2023.
- [6] Yingkai Sha, David John Gagne II, Gregory West, and Roland Stull. Deep-learning-based gridded downscaling of surface meteorological variables in complex terrain. part i: Daily maximum and minimum 2-m temperature. *Journal of Applied Meteorology and Climatology*, 59(12):2057–2073, 2020.
- [7] Yingkai Sha, David John Gagne II, Gregory West, and Roland Stull. Deep-learning-based gridded downscaling of surface meteorological variables in complex terrain. part ii: Daily precipitation. *Journal of Applied Meteorology and Climatology*, 59(12):2075–2092, 2020.



- [8] Xiaohui Zhong, Fei Du, Lei Chen, Zhibin Wang, and Hao Li. Investigating transformer-based models for spatial downscaling and correcting biases of near-surface temperature and wind-speed forecasts. *Quarterly Journal of the Royal Meteorological Society*, 150(758):275–289, 2024.
- [9] Fan Yang, Qiaolin Ye, Kai Wang, and Le Sun. Successful precipitation downscaling through an innovative transformer-based model. *Remote Sensing*, 16(22):4292, 2024.
- [10] Jieli Liu, Chunxiang Shi, Lingling Ge, Ruian Tie, Tao Zhou, Xiaojian Chen, Xiang Gu, Yue Wu, and Zhanfei Shen. A spatial downscaling approach for enhanced accuracy in high wind speed estimation using hybrid attention transformer. *Journal of Meteorological Research*, 39(2):303–321, 2025.
- [11] Yongjian Sun, Kefeng Deng, Kaijun Ren, Jia Liu, Chongjiu Deng, and Yongjun Jin. Deep learning in statistical downscaling for deriving high spatial resolution gridded meteorological data: A systematic review. *ISPRS Journal of Photogrammetry and Remote Sensing*, 208:14–38, 2024.
- [12] Jorge Baño-Medina, Rodrigo Manzananas, and José Manuel Gutiérrez. On the suitability of deep convolutional neural networks for continental-wide downscaling of climate change projections. *Climate Dynamics*, 57(11):2941–2951, 2021.
- [13] Fang Wang, Di Tian, Lisa Lowe, Latif Kalin, and John Lehrter. Deep learning for daily precipitation and temperature downscaling. *Water Resources Research*, 57(4):e2020WR029308, 2021.
- [14] Jérôme Dujardin and Michael Lehning. Wind-topo: Downscaling near-surface wind fields to high-resolution topography in highly complex terrain with deep learning. *Quarterly Journal of the Royal Meteorological Society*, 148(744):1368–1388, 2022.
- [15] Weixin Jin, Yong Luo, Tongwen Wu, Xiaomeng Huang, Wei Xue, and Chaoqing Yu. Deep learning for seasonal precipitation prediction over china. *Journal of Meteorological Research*, 36(2):271–281, 2022.
- [16] Alessandro Damiani, Noriko N Ishizaki, Hidetaka Sasaki, Sarah Feron, and Raul R Cordero. Exploring super-resolution spatial downscaling of several meteorological variables and potential applications for photovoltaic power. *Scientific Reports*, 14(1):7254, 2024.
- [17] Kevin Höhle, Michael Kern, Timothy Hewson, and Rüdiger Westermann. A comparative study of convolutional neural network models for wind field downscaling. *Meteorological Applications*, 27(6):e1961, 2020.
- [18] Antoine Doury, Samuel Somot, Sebastien Gadat, Aurélien Ribes, and Lola Corre. Regional climate model emulator based on deep learning: Concept and first evaluation of a novel hybrid downscaling approach. *Climate Dynamics*, 60(5):1751–1779, 2023.
- [19] Lucy Harris, Andrew TT McRae, Matthew Chantry, Peter D Dueben, and Tim N Palmer. A generative deep learning approach to stochastic downscaling of precipitation forecasts. *Journal of Advances in Modeling Earth Systems*, 14(10):e2022MS003120, 2022.
- [20] Bipin Kumar, Kaustubh Atey, Bhupendra Bahadur Singh, Rajib Chattopadhyay, Nachiketa Acharya, Manmeet Singh, Ravi S Nanjundiah, and Suryachandra A

- Rao. On the modern deep learning approaches for precipitation downscaling. *Earth Science Informatics*, 16(2):1459–1472, 2023.
- [21] Karen Stengel, Andrew Glaws, Dylan Hettinger, and Ryan N King. Adversarial super-resolution of climatological wind and solar data. *Proceedings of the National Academy of Sciences*, 117(29):16805–16815, 2020.
  - [22] Ilenia Manco, Walter Riviera, Andrea Zanetti, Marco Briscolini, Paola Mercogliano, and Antonio Navarra. A new conditional generative adversarial neural network approach for statistical downscaling of the era5 reanalysis over the italian peninsula. *Environmental Modelling & Software*, 188:106427, 2025.
  - [23] Michael Aich, Philipp Hess, Baoxiang Pan, Sebastian Bathiany, Yu Huang, and Niklas Boers. Conditional diffusion models for downscaling & bias correction of earth system model precipitation. *arXiv preprint arXiv:2404.14416*, 2024.
  - [24] Morteza Mardani, Noah D Brenowitz, Yair Cohen, Jaideep Pathak, Chieh-Yu Chen, Cheng-Chin Liu, Arash Vahdat, Karthik Kashinath, Jan Kautz, and Mike Pritchard. Generative residual diffusion modeling for km-scale atmospheric downscaling. *CoRR*, 2023.
  - [25] Fabio Merizzi, Andrea Asperti, and Stefano Colamonaco. Wind speed super-resolution and validation: from era5 to cerra via diffusion models. *Neural Computing and Applications*, 36(34):21899–21921, 2024.
  - [26] Fabio Merizzi, Davide Evangelista, and Harilaos Loukos. Controlling ensemble variance in diffusion models: An application for reanalyses downscaling. *arXiv preprint arXiv:2501.14822*, 2025.
  - [27] Robbie A Watt and Laura A Mansfield. Generative diffusion-based downscaling for climate. *arXiv preprint arXiv:2404.17752*, 2024.
  - [28] Elena Tomasi, Gabriele Franch, and Marco Cristoforetti. Can ai be enabled to perform dynamical downscaling? a latent diffusion model to mimic kilometer-scale cosmo5. 0\_cln9 simulations. *Geoscientific Model Development*, 18(6):2051–2078, 2025.
  - [29] Jieli Liu, Chunxiang Shi, Lingling Ge, Ruian Tie, Xiaojian Chen, Tao Zhou, Xiang Gu, and Zhanfei Shen. Enhanced wind field spatial downscaling method using unet architecture and dual cross-attention mechanism. *Remote Sensing*, 16(11):1867, 2024.
  - [30] Parthiban Loganathan, Elias Zea, Ricardo Vinuesa, and Evelyn Otero. Regional climate projections using a deep-learning-based model-ranking and downscaling framework: Application to european climate zones. *arXiv preprint arXiv:2502.20132*, 2025.
  - [31] Xuanhong Chen, Kairui Feng, Naiyuan Liu, Bingbing Ni, Yifan Lu, Zhengyan Tong, and Ziang Liu. Rainnet: A large-scale imagery dataset and benchmark for spatial precipitation downscaling. *Advances in Neural Information Processing Systems*, 35:9797–9812, 2022.
  - [32] Jieneng Chen, Yongyi Lu, Qihang Yu, Xiangde Luo, Ehsan Adeli, Yan Wang, Le Lu, Alan L Yuille, and Yuyin Zhou. Transunet: Transformers make strong encoders for medical image segmentation. *arXiv preprint arXiv:2102.04306*, 2021.
  - [33] René Ranftl, Alexey Bochkovskiy, and Vladlen Koltun. Vision transformers for dense prediction. In *Proceedings of the IEEE/CVF international conference on*

- computer vision*, pages 12179–12188, 2021.
- [34] Jingyun Liang, Jiezhong Cao, Guolei Sun, Kai Zhang, Luc Van Gool, and Radu Timofte. Swinir: Image restoration using swin transformer. In *Proceedings of the IEEE/CVF international conference on computer vision*, pages 1833–1844, 2021.
  - [35] Zhendong Wang, Xiaodong Cun, Jianmin Bao, Wengang Zhou, Jianzhuang Liu, and Houqiang Li. Uformer: A general u-shaped transformer for image restoration. In *Proceedings of the IEEE/CVF conference on computer vision and pattern recognition*, pages 17683–17693, 2022.
  - [36] Wanfeng Zheng, Qiang Li, Guoxin Zhang, Pengfei Wan, and Zhongyuan Wang. Ittr: Unpaired image-to-image translation with transformers. *arXiv preprint arXiv:2203.16015*, 2022.
  - [37] Lin Zhang, Xinyu Guo, Hongkun Sun, Weigang Wang, and Liwei Yao. Alternate encoder and dual decoder cnn-transformer networks for medical image segmentation. *Scientific Reports*, 15(1):8883, 2025.
  - [38] Michael Crawshaw. Multi-task learning with deep neural networks: A survey. *arXiv preprint arXiv:2009.09796*, 2020.
  - [39] Fenghua Ling, Jing-Jia Luo, Yue Li, Tao Tang, Lei Bai, Wanli Ouyang, and Toshio Yamagata. Multi-task machine learning improves multi-seasonal prediction of the indian ocean dipole. *Nature Communications*, 13(1):7681, 2022.
  - [40] Hang Fan, Xuemin Zhang, Shengwei Mei, Kunjin Chen, and Xinyang Chen. M2gsnet: Multi-modal multi-task graph spatiotemporal network for ultra-short-term wind farm cluster power prediction. *Applied Sciences (Switzerland)*, 10:1–15, 11 2020.
  - [41] Takumi Bannai, Haoyang Xu, Nobuyuki Utsumi, Eunho Koo, Keming Lu, and Hyungjun Kim. Multi-task learning for simultaneous retrievals of passive microwave precipitation estimates and rain/no-rain classification. *Geophysical Research Letters*, 50(7):e2022GL102283, 2023.
  - [42] Pengwei Liu, Wenwei Wang, Bingqing Peng, Binqing Wu, and Liang Sun. Dsaf: A dual-stage adaptive framework for numerical weather prediction downscaling. *arXiv preprint arXiv:2312.12476*, 2023.
  - [43] Zhisheng Lu, Juncheng Li, Hong Liu, Chaoyan Huang, Linlin Zhang, and Tieyong Zeng. Transformer for single image super-resolution. In *Proceedings of the IEEE/CVF conference on computer vision and pattern recognition*, pages 457–466, 2022.
  - [44] Yifeng Yang, Hengqian Zhao, Xiadan Huangfu, Zihan Li, and Pan Wang. Vit-isrgan: A high-quality super-resolution reconstruction method for multispectral remote sensing images. *IEEE Journal of Selected Topics in Applied Earth Observations and Remote Sensing*, 18:3973–3988, 2025.
  - [45] Jiezhong Cao, Yawei Li, Kai Zhang, and Luc Van Gool. Video super-resolution transformer. *arXiv preprint arXiv:2106.06847*, 2021.
  - [46] Huan Liu, Mingwen Shao, Chao Wang, and Feilong Cao. Image super-resolution using a simple transformer without pretraining. *Neural Processing Letters*, 55(2):1479–1497, 2023.
  - [47] Sixiao Zheng, Jiachen Lu, Hengshuang Zhao, Xiatian Zhu, Zekun Luo, Yabiao Wang, Yanwei Fu, Jianfeng Feng, Tao Xiang, Philip HS Torr, et al. Rethinking

- semantic segmentation from a sequence-to-sequence perspective with transformers. In *Proceedings of the IEEE/CVF conference on computer vision and pattern recognition*, pages 6881–6890, 2021.
- [48] Dan Hendrycks and Kevin Gimpel. Gaussian error linear units (gelus). *arXiv preprint arXiv:1606.08415*, 2016.
  - [49] Yuxin Wu and Kaiming He. Group normalization. 3 2018.
  - [50] Augustus Odena, Vincent Dumoulin, and Chris Olah. Deconvolution and checkerboard artifacts. *Distill*, 1(10):e3, 2016.
  - [51] Mario Lucic, Karol Kurach, Marcin Michalski, Sylvain Gelly, and Olivier Bousquet. Are gans created equal? a large-scale study. *Advances in neural information processing systems*, 31, 2018.
  - [52] Joelle Pineau, Philippe Vincent-Lamarre, Koustuv Sinha, Vincent Larivière, Alina Beygelzimer, Florence d’Alché Buc, Emily Fox, and Hugo Larochelle. Improving reproducibility in machine learning research (a report from the neurips 2019 reproducibility program). *Journal of machine learning research*, 22(164):1–20, 2021.
  - [53] Zachary C Lipton and Jacob Steinhardt. Troubling trends in machine learning scholarship: Some ml papers suffer from flaws that could mislead the public and stymie future research. *Queue*, 17(1):45–77, 2019.
  - [54] Ilya Loshchilov and Frank Hutter. Decoupled weight decay regularization. *arXiv preprint arXiv:1711.05101*, 2017.
  - [55] Andrea Asperti, Fabio Merizzi, Alberto Paparella, Giorgio Pedrazzi, Matteo Angelinelli, and Stefano Colamonaco. Precipitation nowcasting with generative diffusion models. *Applied Intelligence*, 55(2):1–21, 2025.
  - [56] Qidong Yang, Alex Hernandez-Garcia, Paula Harder, Venkatesh Ramesh, Prasanna Sattigeri, Daniela Szwarcman, Campbell D Watson, and David Rolnick. Fourier neural operators for arbitrary resolution climate data downscaling. *Journal of Machine Learning Research*, 25(420):1–30, 2024.
  - [57] Paula Harder, Alex Hernandez-Garcia, Venkatesh Ramesh, Qidong Yang, Prasanna Sattigeri, Daniela Szwarcman, Campbell Watson, and David Rolnick. Hard-constrained deep learning for climate downscaling. *Journal of Machine Learning Research*, 24(365):1–40, 2023.